A sphere region tracking control scheme for underwater vehicles

Xing Liu, Mingjun Zhang, Zhenzhong Chu and Eric Rogers

***Abstract*—The concept of region tracking control has advantages for underwater vehicles for some special missions, such as pipeline tracking. This paper develops a sphere region tracking control scheme based on barrier Lyapunov functions, where an observer is used to estimate the effects of external disturbances and modeling uncertainty. It is shown that the distance between the vehicle's position and the corresponding point on the desired trajectory is always kept within the prescribed boundaries. Simultaneously, the absolute value of each attitude-tracking error is less than another defined boundary. Finally, the new control scheme is applied to a fully actuated underwater vehicle, and the advantages of this strategy are validated compared to other region-tracking control schemes.**

***Index Terms*—Underwater vehicle, sphere region tracking, observer, barrier Lyapunov function, prescribed boundaries.**

I. Introduction

ONE view of an underwater vehicle is as a platform to carry sensors or manipulators to perform different missions [1]–[4], including underwater observation, underwater searching, and even underwater operation. A high-performance control system enables an underwater vehicle to complete a given mission. Examples of control algorithms applied to underwater vehicles include sliding mode control, e.g., [5], model predictive control [6], [7], neural network, or fuzzy-based control [8]. In these cited references, the control objective is to command the vehicle to have the highest possible tracking accuracy.

This paper considers region tracking control for an underwater vehicle applicable to missions where the objective is to keep the tracking error within prescribed boundaries, especially in steady-state operation. An example area is pipeline tracking, where, given the detection range of sensors, a more applicable objective is that the distance between the vehicle's position and the corresponding point on the desired trajectory is less than a prescribed boundary, coupled with limiting the attitude errors to within the prescribed boundaries. Moreover, cases may arise where the tracking error must be within the specified boundaries in finite time, and any overshoot on any Degree of Freedom (DOF) must be less than a specified value.

Manuscript received xx xx, xx; revised xx xx, xx. This work is supported by the National Natural Science Foundation of China under Grant 51839004, 52201357 and Fundamental Research Funds for the Central Universities under Grant 3072022TS0701.

Xing Liu and Mingjun Zhang are with College of Mechanical and Electrical Engineering, Harbin Engineering University, Harbin, 150001, China. e-mail: liuxing20080724@gmail.com.

Zhenzhong Chu is with School of Mechanical Engineering, University of Shanghai for Science and Technology, Shanghai, 200093, China.

Eric Rogers is with the School of Electronics and Computer Science, University of Southampton, Southampton SO17 1BJ, UK.

Previous research, e.g., [9], developed a region-tracking control scheme for an underwater vehicle. Potential energy functions were designed based on the prescribed boundaries and the region error variable used to derive the control law. This research focused on the tracking error's region performance in the steady state and did not consider this characteristic during the transient stage. Barrier Lyapunov function-based control has been developed for systems with state constraints, and there is previous research on their application to underwater vehicle tracking control. For example, a singularity-free controller was designed for surface vessels to satisfy the predefined performance requirements using a logarithmic barrier function in [10]. In [11], a saturated adaptive robust neural network control based on reinforcement learning for underactuated AUVs was developed, where a prescribed performance-bound method is used to improve the tracking accuracy. Moreover, in [12], an adaptive neural network control using the barrier Lyapunov function and a modified line-of-sight guidance law developed for marine vehicles with state and input constraints, where the uniform ultimate boundedness of the closed-loop system was verified. Another application of prescribed performance control is for an AUV operating in formation, where a limited communication range is considered, together with a need to ensure collision avoidance, see, e.g., [13].

Barrier Lyapunov function-based control is a good choice for designing a region tracking controller since it can obtain the tracking performance with the predesigned transient and steady-state performance, e.g., [14]–[18]. However, these barrier Lyapunov function-based controllers focus on improving the tracking precision under state constraints. In general terms, region tracking control aims to steer the vehicle within the prescribed boundaries, but high precision would require using control inputs that would have detrimental effects on thrusters. Moreover, navigation sensors in underwater vehicles may not provide the accuracy necessary to achieve the control objectives. In [19] and [20], investigated the adaptive region tracking control problem with the prescribed transient performance for underwater vehicles based on defined performance control. Specifically, the tracking error for each DOF in [19] was changed between the prescribed boundaries by combining a barrier function and a piecewise smooth Lyapunov function. Alternatively, in [20], the tracking error was varied between the specified limits by adding a nonlinear transformation to the tracking error for each DOF under a defined performance control design.

For some underwater missions, e.g., the pipeline tracking application discussed above, it would be more applicable that

the distance between the vehicle's position and the corresponding point on the desired trajectory is less than a prescribed value and the attitude errors are within specified values. This paper develops new results on region tracking control for underwater vehicles for this requirement. The main novel contributions of this paper are: i) a region tracking control scheme is developed by designing two barrier Lyapunov functions with the norm of the position tracking error and the absolute value of the attitude error, which is different from [19] and [20] where the region tracking control on each DOF is achieved based on the corresponding element of the tracking error, ii) in the new design, an observer estimates the uncertainty, including external disturbances and the modeling uncertainty, based on the boundedness of the uncertainty and its derivative, and the associated estimation error converges to zero in a finite time, iii) it is proved that the norm of the position tracking error is less than a prescribed value, coupled with attitude tracking errors that also are within prescribed boundaries under the new control scheme, and iv) as a necessary first step in evaluating the performance of new design, it is applied (in simulation) to an open-frame underwater vehicle subject to ocean current and other external disturbances. The comparative results demonstrate the effectiveness of the new design.

The rest of this paper begins with the problem formulation in Section II. Section III gives the development of the new design, including the stability proof. Simulation-based case studies are given in Section IV. Finally, the main new results in this paper are summarized in the last section, together with a discussion of possible future research areas.

II. Problem Formulation

Fig.1 gives the frames associated with an underwater vehicle, including the inertial frame $E = (X_e, Y_e, Z_e)$ and the body-fixed frame $B = (X_b, Y_b, Z_b)$. The location of the vehicle in the inertial frame is defined by $\eta_1 = (x, y, z)^T$, and the attitude (Euler angles) of the vehicle is described by $\eta_2 = (\phi, \theta, \psi)^T$ with roll (ϕ), pitch (θ) and yaw (ψ) in the inertial frame. The vector $\upsilon = (\upsilon_x, \upsilon_y, \upsilon_z)^T$ represents the linear velocity in the body-fixed frame and $\omega = (\omega_\phi, \omega_\theta, \omega_\psi)^T$ the angular velocity in the body-fixed frame.

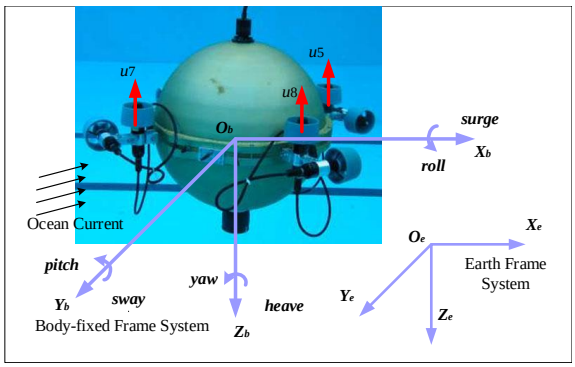

Fig. 1. Coordinate frames, see [21]

The relationship between the location and the linear velocity vectors can be written in the form (see [22])

$$\dot{\eta}_1 = \mathbf{R}_\mathbf{B}^\mathbf{E} \upsilon$$
$$\mathbf{R}_\mathbf{B}^\mathbf{E} = \begin{bmatrix} C_\psi C_\theta & C_\psi S_\theta S_\phi - S_\psi C_\phi & C_\psi S_\theta C_\phi + S_\psi S_\phi \\ S_\psi C_\theta & S_\psi S_\theta S_\phi + C_\psi C_\phi & S_\psi S_\theta C_\phi - C_\psi S_\phi \\ -S_\theta & C_\theta S_\phi & C_\theta C_\phi \end{bmatrix} \tag{1}$$

where $\mathbf{R}_\mathbf{B}^\mathbf{E}$ is the translation matrix from the body-fixed frame B to the inertial frame E, $C_k = \cos(k)$ and $S_k = \sin(k)$, for $k = \psi$, ϕ, or θ. Similarly, the relationship between the Euler angles and the angular velocity vector is, see [22],

$$\dot{\eta}_2 = \mathbf{R_2} \omega$$
$$\mathbf{R_2} = \begin{bmatrix} 1 & S_\phi T_\theta & C_\phi T_\theta \\ 0 & C_\phi & -S_\phi \\ 0 & S_\phi / C_\theta & C_\phi / C_\theta \end{bmatrix} \tag{2}$$

where $T_\theta = \tan(\theta)$. The matrix R_2 has a potential singularity, i.e., when the pitch angle (θ) is $\frac{\pi}{2}$ or $-\frac{\pi}{2}$. However, in general, the pitch angle (θ) is always far away from the neighborhood of $\frac{\pi}{2}$ or $-\frac{\pi}{2}$ due to the structural design of the vehicle.

From [22], the translational and rotational dynamics of the vehicle can be written as

$$\begin{aligned} \mathbf{M_1} \dot{\upsilon} + \mathbf{C_1}(\upsilon_r, \omega_r)\upsilon_r + \mathbf{D_1}(\upsilon_r)\upsilon_r + \mathbf{g_1}(\eta_\mathbf{2}) &= \tau_\mathbf{1} \\ \mathbf{M_2} \dot{\omega}_r + \mathbf{C_2}(\upsilon_r, \omega_r)\omega_r + \mathbf{D_2}(\omega_r)\omega_r + \mathbf{g_2}(\eta_\mathbf{2}) &= \tau_2 \end{aligned} \tag{3}$$

where $\mathbf{M_1}$ and $\mathbf{M_2}$ are the 3×3 inertia matrices, including the added mass terms; $\mathbf{C_1}(\upsilon_r, \omega_r)$ and $\mathbf{C_2}(\upsilon_r, \omega_r)$ are the 3×3 matrixes of the centrifugal and Coriolis terms; υ_r and ω_r are the linear and angular velocities relative to the ocean current in the body-fixed frame, respectively; $\mathbf{D_1}(\upsilon_r)$ and $\mathbf{D_2}(\omega_r)$ are the matrices representing the hydrodynamic drag terms; $\mathbf{g_1}(\eta_\mathbf{2})$ and $\mathbf{g_2}(\eta_\mathbf{2})$ are 3×1 vectors of the restoring forces; and τ_1 and τ_2 are 3×1 vectors, respectively, describing forces and moments supplied by thrusters to the vehicle.

It is assumed that the entries in this vehicle model are available from modeling or experimental method studies, such as the towing-tank method given in [23]. However, modeling uncertainties will still be present. In addition, the vehicle moves under the influence of an irrotational current, whose effects can be modeled as additive external disturbances acting on the dynamics described by (3). Including representations of both these effects results in the following model for analysis and design:

$$\begin{aligned} \hat{\mathbf{M}}_\mathbf{1} \dot{\upsilon} + \hat{\mathbf{C}}_\mathbf{1}(\upsilon, \omega)\upsilon + \hat{\mathbf{D}}_\mathbf{1}(\upsilon)\upsilon + \hat{\mathbf{g}}_\mathbf{1}(\eta_2) &= \tau_1 + \tau_{d1} \\ \hat{\mathbf{M}}_\mathbf{2} \dot{\omega} + \hat{\mathbf{C}}_\mathbf{2}(\upsilon, \omega)\omega + \hat{\mathbf{D}}_\mathbf{2}(\omega)\omega + \hat{\mathbf{g}}_\mathbf{2}(\eta_2) &= \tau_2 + \tau_{d2} \end{aligned} \tag{4}$$

where for a variable, say H, $\hat{H}$ denotes its estimate, τ_{d1} and τ_{d2} are 3×1 vectors representing the modelling uncertainties and the external disturbances, respectively. It is assumed that there exist unknown upper bounds $\bar{\rho}_{h1} > 0$ and $\bar{\rho}_{h2} > 0$ such that $\|\tau_{d1}\| < \bar{\rho}_{h1}$ and $\|\tau_{d2}\| < \bar{\rho}_{h2}$ (where $\|\cdot\|$ denotes an appropriately chosen norm). Furthermore, it is assumed that the first derivatives with respect to time of τ_{d1} and τ_{d2} exist,

and satisfy bounds of the form $\|\dot{\tau}_{d1}\| < \bar{\rho}_{H1}$ and $\|\dot{\tau}_{d2}\| < \bar{\rho}_{H2}$ for unknown positive constants $\bar{\rho}_{H1}$ and $\bar{\rho}_{H2}$.

This paper considers region tracking control, particularly the scenario shown in Fig. 2. The core objective is to steer the vehicle within the desired trajectory's prescribed upper and lower boundaries, but not to (always) enforce zero tracking error. One approach to this problem for attitude control would be to design a region tracking controller for each DOF. Such a control strategy assumes no interaction between the axes. If this is not the case then the alternative is to design a region tracking controller based on the distance between the center of the vehicle at any time instant and the corresponding point on the desired trajectory, as measured by the associated norm. In this paper, DBCD denotes this distance.

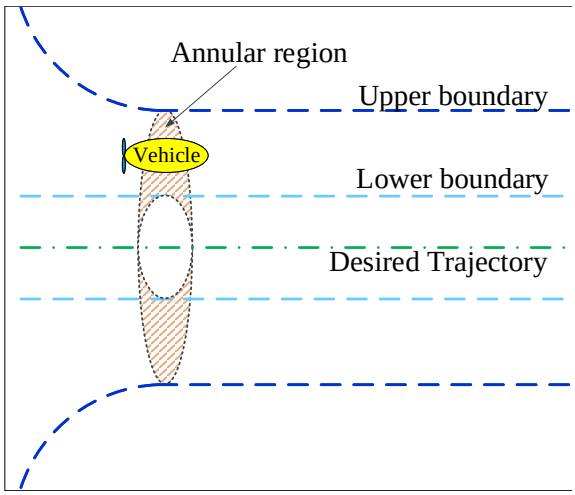

Fig. 2. Schematic of the region tracking control considered.

The new design is relevant to applications with a limited communication range or a limited detection range of the sensors. In such cases, the distance between the actual and target trajectories must be less than a prescribed value. There have been previous region-based control designs, and in this paper, comparative studies of the new design against alternatives are given based on the model of an actual vehicle. These results are simulation-based and are an essential step before experimental validation can be planned.

The following lemma will be used in the control design.

Lemma 1. *[15] Consider a nonlinear system $\dot{x} = f(x)$. Then if there exists a Lyapunov function $V(x)$ such that $\dot{V}(x) \leq -c_1 V(x) + \vartheta_1$ with positive scalars c_1 and ϑ_1, the nonlinear system is exponentially convergent and the Lyapunov function $V(x)$ is bounded.*

III. Control Design

This section develops the new control scheme with the objectives given in Section II. In particular, two forms of Lyapunov functions are used to undertake a stability analysis and design the region tracking control law by using the backstepping technique. Moreover, the terms τ_{d1} and τ_{d2} in (4) are estimated by a nonlinear observer.

A. Barrier Lyapunov functions

Given the desired trajectory $\eta_d = [\eta_{d1}^T, \eta_{d2}^T]^T$, define the position tracking error as $\mathbf{z}_{a1} = \eta_1 - \eta_{d1}$ and the attitude tracking error as $\mathbf{z}_2 = \eta_2 - \eta_{d2}$. For the first control objective, i.e., to guarantee that the distance DBCD is kept within the prescribed boundaries, a Lyapunov function on the set $\left(\sqrt{\varepsilon_{1b}}, \sqrt{\varepsilon_{1a}}\right)$ is used of the form

$$V_1 = \frac{\left(\|\mathbf{z}_{a1}\|^2 - m_\mu\right)^2}{\left(\varepsilon_{1a} - \|\mathbf{z}_{a1}\|^2\right)\left(\|\mathbf{z}_{a1}\|^2 - \varepsilon_{1b}\right)} \tag{5}$$

where $\varepsilon_{1b} > 0$ is a suitably small parameter, $\sqrt{\varepsilon_{1a}} = \rho_{\infty 1} + (\rho_{01} - \rho_{\infty 1})\, e^{-\lambda_1 t}$ with positive design parameters ρ_{01}, $\rho_{\infty 1}$, λ_1, $m_\mu = \frac{1}{2}(\varepsilon_{1a} + \varepsilon_{1b})$, and $\|\mathbf{z}_{a1}\|^2 = \mathbf{z}_{a1}^T \mathbf{z}_{a1}$. Also, it is required that $\rho_{\infty 1} > \rho_{01}$ and $\varepsilon_{1a}(0) > \|\mathbf{z}_{a1}(0)\|^2 > \varepsilon_{1b}$.

Remark 1. *It is routine to establish that the Lyapunov function V_1 is continuous and bounded on the set $\left(\sqrt{\varepsilon_{1b}}, \sqrt{\varepsilon_{1a}}\right)$. Also when $\|\mathbf{z}_{a1}\|^2 \to \varepsilon_{1b}$ or ε_{1a}, $V_1 \to \infty$. If the boundedness of the Lyapunov function is verified, the norm of the position tracking error, i.e., DBCD, is limited to within the prescribed boundaries.*

The partial derivative of the Lyapunov function V_1 with respect to $\|\mathbf{z}_{a1}\|^2$, denoted by $\frac{\partial}{\partial \|\mathbf{z}_{a1}\|^2} V_1$, can be written as

$$\begin{aligned}\frac{\partial}{\partial \|\mathbf{z}_{a1}\|^2} V_1 &= \frac{\left(\|\mathbf{z}_{a1}\|^2 - m_\mu\right)\left(\frac{\varepsilon_{1a}^2 + \varepsilon_{1b}^2}{2} - \varepsilon_{1a}\varepsilon_{1b}\right)}{\left(\left(\varepsilon_{1a} - \|\mathbf{z}_{a1}\|^2\right)\left(\|\mathbf{z}_{a1}\|^2 - \varepsilon_{1b}\right)\right)^2} \\ &= \frac{C_a\left(\|\mathbf{z}_{a1}\|^2 - m_\mu\right)}{\left(\left(\varepsilon_{1a} - \|\mathbf{z}_{a1}\|^2\right)\left(\|\mathbf{z}_{a1}\|^2 - \varepsilon_{1b}\right)\right)^2}\end{aligned} \tag{6}$$

where $C_a = \left(\frac{\varepsilon_{1a}^2 + \varepsilon_{1b}^2}{2} - \varepsilon_{1a}\varepsilon_{1b}\right) > 0$. Also $\frac{\partial}{\partial \|\mathbf{z}_{a1}\|^2} V_1$ has the following property:

$$\begin{aligned}&\frac{(\varepsilon_{1a} + \varepsilon_{1b})\left(\|\mathbf{z}_{a1}\|^2 - m_\mu\right)\|\mathbf{z}_{a1}\|^2}{C_a} \frac{\partial}{\partial \|\mathbf{z}_{a1}\|^2} V_1 - V_1 \\ &= \frac{\left(\|\mathbf{z}_{a1}\|^2 - m_\mu\right)^2\left(\|\mathbf{z}_{a1}\|^4 + \varepsilon_{1a}\varepsilon_{1b}\right)}{\left(\left(\varepsilon_{1a} - \|\mathbf{z}_{a1}\|^2\right)\left(\|\mathbf{z}_{a1}\|^2 - \varepsilon_{1b}\right)\right)^2} \geq 0\end{aligned} \tag{7}$$

Taking the partial derivative of V_1 with respect to ε_{1a} gives

$$\begin{aligned}\frac{\partial}{\partial \varepsilon_{1a}} V_1 &= \frac{-(\varepsilon_{1a} - \varepsilon_{1b})\left(\|\mathbf{z}_{a1}\|^2 - m_\mu\right)\left(\|\mathbf{z}_{a1}\|^2 - \varepsilon_{1b}\right)}{2\left(\left(\varepsilon_{1a} - \|\mathbf{z}_{a1}\|^2\right)\left(\|\mathbf{z}_{a1}\|^2 - \varepsilon_{1b}\right)\right)^2} \\ &= -\frac{(\varepsilon_{1a} - \varepsilon_{1b})\left(\|\mathbf{z}_{a1}\|^2 - \varepsilon_{1b}\right)}{2C_a} \frac{\partial}{\partial \|\mathbf{z}_{a1}\|^2} V_1\end{aligned} \tag{8}$$

and to keep the attitude tracking error for each DOF within the prescribed boundaries, the following Lyapunov function on the set $\left(-\sqrt{\varepsilon_{2a}}, \sqrt{\varepsilon_{2a}}\right)$ is used:

$$V_2 = \sum_{i=1}^{3} \frac{\mathbf{z}_{2i}^2}{\varepsilon_{2a} - \mathbf{z}_{2i}^2} \tag{9}$$

where $\mathbf{z}_{2i}$ is the ith entry of the attitude tracking error $\mathbf{z}_2$. In this paper, the prescribed boundaries are identical for roll, pitch and yaw tracking, and $\sqrt{\varepsilon_{2a}} = \rho_{\infty 2} + (\rho_{02} - \rho_{\infty 2})\, e^{-\lambda_2 t}$ with positive design parameters ρ_{02}, $\rho_{\infty 2}$ and λ_2. It is also required that $\varepsilon_{2a} > \mathbf{z}_{2i}^2(0)$.

Taking the partial derivative of the Lyapunov function V_2 with respect to $\mathbf{z}_{2i}^2$ and ε_{2a}, respectively, gives

$$\begin{aligned} \frac{\partial}{\partial \mathbf{z}_{2i}^2} V_2 &= \frac{\varepsilon_{2a}}{\left(\varepsilon_{2a} - \mathbf{z}_{2i}^2\right)^2} > 0 \\ \frac{\partial}{\partial \varepsilon_{2a}} V_2 &= \sum_{i=1}^{3} \frac{-\mathbf{z}_{2i}^2}{\left(\varepsilon_{2a} - \mathbf{z}_{2i}^2\right)^2} = -\sum_{i=1}^{3} \frac{\mathbf{z}_{2i}^2}{\varepsilon_{2a}} \frac{\partial}{\partial \mathbf{z}_{2i}^2} V_2 \end{aligned} \tag{10}$$

Also, $\frac{\partial}{\partial \mathbf{z}_{2i}^2} V_2$ has the property that:

$$2\sum_{i=1}^{3} \mathbf{z}_{2i}^2 \frac{\partial}{\partial \mathbf{z}_{2i}^2} V_2 - V_2 = \sum_{i=1}^{3} \frac{\mathbf{z}_{2i}^4 + \varepsilon_{2a}\mathbf{z}_{2i}^2}{\left(\varepsilon_{2a} - \mathbf{z}_{2i}^2\right)^2} \geq 0 \tag{11}$$

Given the desired trajectory, define the linear velocity tracking error as $\mathbf{z}_3 = \upsilon - \alpha_1$ and the angular velocity error as $\mathbf{z}_4 = \omega - \alpha_2$, where α_1 and α_2 are the virtual control vectors, designed below. The time derivatives of the Lyapunov functions V_1 and V_2, respectively, are

$$\begin{aligned} \dot{V}_1 =& -\left(\frac{\partial}{\partial \|\mathbf{z}_{a1}\|^2} V_1\right) \frac{\left(\varepsilon_{1a} - \varepsilon_{1b}\right)\left(\|\mathbf{z}_{a1}\|^2 + \varepsilon_{1b}\right)}{2C_a} \dot{\varepsilon}_{1a} \\ &+ 2\left(\frac{\partial}{\partial \|\mathbf{z}_{a1}\|^2} V_1\right) \mathbf{z}_{a1}^T \dot{\mathbf{z}}_{a1} \\ =& \, 2\left(\frac{\partial}{\partial \|\mathbf{z}_{a1}\|^2} V_1\right) \mathbf{z}_{a1}^T \left(\mathbf{R}_{\mathbf{B}}^{\mathbf{E}} \left(\mathbf{z_3} + \alpha_{\mathbf{1}}\right) - \dot{\eta}_{\mathbf{d1}}\right) \\ &- \left(\frac{\partial}{\partial \|\mathbf{z}_{a1}\|^2} V_1\right) \frac{\left(\varepsilon_{1a} - \varepsilon_{1b}\right)\left(\|\mathbf{z}_{a1}\|^2 + \varepsilon_{1b}\right)}{2C_a} \dot{\varepsilon}_{1a} \end{aligned} \tag{12}$$

$$\begin{aligned} \dot{V}_2 =& \, 2\sum_{i=1}^{3} \frac{\partial}{\partial \mathbf{z}_{2i}^2} V_2 \mathbf{z}_{2i} \dot{\mathbf{z}}_{2i} + \left(\frac{\partial}{\partial \varepsilon_{2a}} V_2\right) \dot{\varepsilon}_{2a} \\ =& \, 2\sum_{i=1}^{3} \frac{\partial}{\partial \mathbf{z}_{2i}^2} V_2 \mathbf{z}_2^T \left(\mathbf{R_2}\left(\mathbf{z_4} + \alpha_{\mathbf{2}}\right) - \dot{\eta}_{\mathbf{d2}}\right) \\ &- \sum_{i=1}^{3} \frac{\partial}{\partial \mathbf{z}_{2i}^2} V_2 \frac{\mathbf{z}_{2i}^2}{\varepsilon_{2a}} \dot{\varepsilon}_{2a} \end{aligned} \tag{13}$$

To achieve $\dot{V}_1 < 0$ and $\dot{V}_2 < 0$, the virtual control vectors α_1 and α_1 are, respectively, chosen as:

$$\begin{aligned} \alpha_1 =& \, \mathbf{R}_{\mathbf{B}}^{\mathbf{E}\,-1} \left(\dot{\eta}_{d1} + \frac{\left(\varepsilon_{1a} - \varepsilon_{1b}\right)\left(\|\mathbf{z}_{a1}\|^2 - \varepsilon_{1b}\right)\dot{\varepsilon}_{1a}}{2C_a\|\mathbf{z}_{a1}\|^2} \mathbf{z}_{a1}\right) \\ &- \mathbf{R}_{\mathbf{B}}^{\mathbf{E}\,-1} \left(\frac{\left(\varepsilon_{1a} + \varepsilon_{1b}\right)\left(\|\mathbf{z}_{a1}\|^2 - m_\mu\right)}{2C_a} \mathbf{z}_{a1}\right) \\ &+ \mathbf{R}_{\mathbf{B}}^{\mathbf{E}\,-1} \left(\left(\frac{\partial}{\partial \|\mathbf{z}_{a1}\|^2} V_1\right) \frac{\mathbf{z}_{a1}}{2}\right) \end{aligned} \tag{14}$$

$$\alpha_2 = \mathbf{R}_{\mathbf{2}}^{-\mathbf{1}} \left(\dot{\eta}_{\mathbf{d2}} + \frac{\dot{\varepsilon}_{\mathbf{2a}}}{\mathbf{2}\varepsilon_{\mathbf{2a}}} \mathbf{z_2} - \mathbf{z_2} - \mathbf{diag}\left(\frac{\partial}{\partial \mathbf{z}_{\mathbf{2i}}^{\mathbf{2}}} \mathbf{V}\right) \frac{\mathbf{z_2}}{\mathbf{2}}\right) \tag{15}$$

Substituting the virtual control vectors α_1 and α_1 into (12) and (13), respectively, simplifies $\dot{V}_1$ and $\dot{V}_2$ to

$$\begin{aligned} \dot{V}_1 =& \, 2\left(\frac{\partial}{\partial \|\mathbf{z}_{a1}\|^2} V_1\right) \mathbf{z}_{a1}^T \mathbf{R}_B^E \mathbf{z}_3 - \left(\frac{\partial}{\partial \|\mathbf{z}_{a1}\|^2} V_1\right)^2 \mathbf{z}_{a1}^T \mathbf{z}_{a1} \\ &- \left(\frac{\partial}{\partial \|\mathbf{z}_{a1}\|^2} V_1\right) \frac{\left(\varepsilon_{1a} + \varepsilon_{1b}\right)\left(\|\mathbf{z}_{a1}\|^2 - m_\mu\right)}{C_a} \mathbf{z}_1^T \mathbf{z}_{a1} \\ \leq& -V_1 + 2\left(\frac{\partial}{\partial \|\mathbf{z}_{a1}\|^2} V_1\right) \mathbf{z}_{a1}^T \mathbf{R}_B^E \mathbf{z}_3 \\ &- \left(\frac{\partial}{\partial \|\mathbf{z}_{a1}\|^2} V_1\right)^2 \mathbf{z}_{a1}^T \mathbf{z}_{a1} \end{aligned} \tag{16}$$

$$\begin{aligned} \dot{V}_2 =& \, 2\sum_{i=1}^{3} \frac{\partial}{\partial \mathbf{z}_{2i}^2} V_2 \mathbf{z}_2 \mathbf{z}_2^T R_2 \mathbf{z}_4 - 2\sum_{i=1}^{3} \frac{\partial}{\partial \mathbf{z}_{2i}^2} V_2 \mathbf{z}_{2i}^2 \\ &- \sum_{i=1}^{3} \left(\frac{\partial}{\partial \mathbf{z}_{2i}^2} V_2\right)^2 \mathbf{z}_{2i}^2 \\ \leq& \, 2\sum_{i=1}^{3} \frac{\partial}{\partial \mathbf{z}_{2i}^2} V_2 \mathbf{z}_2 \mathbf{z}_2^T R_2 \mathbf{z}_4 - V_2 - \sum_{i=1}^{3} \left(\frac{\partial}{\partial \mathbf{z}_{2i}^2} V_2\right)^2 \mathbf{z}_{2i}^2 \end{aligned} \tag{17}$$

B. Nonlinear observer design

To derive the region tracking control law, the unknown terms τ_{d1} and τ_{d2} in (4) must be estimated. Given (4) and full-state measurements, the nonlinear observer used has the form:

$$\begin{aligned} \dot{\hat{\upsilon}} =& \, \hat{\mathbf{M}}_1^{-1}\tau_1 - \hat{\mathbf{M}}_1^{-1}\left(\hat{\mathbf{C}}_1(\upsilon,\omega)\,\upsilon + \hat{\mathbf{D}}_1(\upsilon)\,\upsilon + \hat{\mathbf{g}}_1(\eta_2)\right) \\ &+ \hat{\mathbf{d}}_1(t) + k_1|\tilde{\upsilon}|^{0.5} sign(\tilde{\upsilon}) + k_2\tilde{\upsilon} \\ \dot{\hat{\mathbf{d}}}_1(t) =& \, k_3 sign(\tilde{\upsilon}) + k_4\tilde{\upsilon} \end{aligned} \tag{18}$$

$$\begin{aligned} \dot{\hat{\omega}} =& \, \hat{\mathbf{M}}_2^{-1}\tau_2 - \hat{\mathbf{M}}_2^{-1}\left(\hat{\mathbf{C}}_2(\upsilon,\omega)\,\omega + \hat{\mathbf{D}}_2(\omega)\,\omega + \hat{\mathbf{g}}_2(\eta_2)\right) \\ &+ \hat{\mathbf{d}}_2(t) + p_1|\tilde{\omega}|^{0.5} sign(\tilde{\omega}) + p_2\tilde{\omega} \\ \dot{\hat{\mathbf{d}}}_2(t) =& \, p_3 sign(\tilde{\omega}) + p_4\tilde{\omega} \end{aligned} \tag{19}$$

where $\hat{\mathbf{d}}_1(t)$ and $\hat{\mathbf{d}}_2(t)$ are, respectively, the estimates of $\mathbf{d}_1(t) = \hat{\mathbf{M}}_1^{-1}\tau_{d1}$ and $\mathbf{d}_2(t) = \hat{\mathbf{M}}_2^{-1}\tau_{d2}$. $\hat{\upsilon}$ and $\hat{\omega}$ are, respectively, the estimates of υ and ω. $\tilde{\upsilon} = \upsilon - \hat{\upsilon}$, and $\tilde{\omega} = \omega - \hat{\omega}$. $k_i, i = 1,2,3,4$ and $p_i, i = 1,2,3,4$, are positive scalars that satisfy

$$\begin{aligned} &k_1 > 2\sqrt{\rho_{H1}}, k_2 > 0 \\ &k_3 > \rho_{H1}, k_4 > \frac{4k_2^2\left(9k_1^2 + 10k_3 - 10\rho_{H1}\right)}{k_3 - \rho_{H1}} \\ &p_1 > 2\sqrt{\rho_{H2}}, p_2 > 0 \\ &p_3 > \rho_{H2}, p_4 > \frac{4p_2^2\left(9p_1^2 + 10p_3 - 10\rho_{H2}\right)}{p_3 - \rho_{H2}} \end{aligned} \tag{20}$$

Remark 2. *Although the terms of $\dot{\mathbf{d}}_1$ and $\dot{\mathbf{d}}_2$ are bounded, their bounds are not known a priori. In the observer, the parameters k_i and p_i are determined by these bounds. One simple way is to choose k_i and p_i by trial and error.*

Define $\tilde{\mathbf{d}}_1(t) = \mathbf{d}_1(t) - \hat{\mathbf{d}}_1(t)$ and $\tilde{\mathbf{d}}_2(t) = \mathbf{d}_2(t) - \hat{\mathbf{d}}_2(t)$. Then using (4), (18) and (19), the dynamics of the estimated errors $\tilde{\mathbf{d}}_\mathbf{1}$ and $\tilde{\mathbf{d}}_\mathbf{2}$ are given by

$$\begin{aligned} \dot{\tilde{\upsilon}} &= -k_1|\tilde{\upsilon}|^{0.5} sign(\tilde{\upsilon}) - k_2\tilde{\upsilon} + \tilde{\mathbf{d}}_1(t) \\ \dot{\tilde{\mathbf{d}}}_1(t) &= \dot{\mathbf{d}}_1(t) - k_3 sign(\tilde{\upsilon}) - k_4\tilde{\upsilon} \end{aligned} \tag{21}$$

$$\begin{aligned} \dot{\tilde{\omega}} &= -p_1|\tilde{\omega}|^{0.5} sign(\tilde{\omega}) - p_2\tilde{\omega} + \tilde{\mathbf{d}}_2(t) \\ \dot{\tilde{\mathbf{d}}}_2(t) &= \dot{\mathbf{d}}_2(t) - p_3 sign(\tilde{\omega}) - p_4\tilde{\omega} \end{aligned} \tag{22}$$

Using results in [24], it can be shown that the estimation errors $\tilde{\mathbf{d}}_1$ and $\tilde{\mathbf{d}}_2$ converge to zero in a finite time. The stability analysis can be found in [24].

C. Control law and stability analysis

Consider the Lyapunov function:

$$V_T = \frac{1}{2}\mathbf{z_3^T z_3} + \frac{\mathbf{1}}{\mathbf{2}}\mathbf{z_4^T z_4} + \mathbf{V_1} + \mathbf{V_2} \tag{23}$$

Then the following is the main result of this paper.

Theorem 1. *Consider the underwater vehicle's dynamics* (1) *with modelling uncertainty and external disturbances, and suppose that the initial conditions of the vehicle satisfy the constraints $\varepsilon_{1a}(0) > \|\mathbf{z}_{a1}(0)\|^2 > \varepsilon_{1b}$ and $\varepsilon_{2a} > \mathbf{z}_{2i}^2(0)$. Suppose also that the nonlinear observer* (18) *and* (19) *is used to estimate the general uncertainty, including unknown external disturbance and modeling uncertainty, and the control law is given by*

$$\begin{aligned} \tau_1 = \hat{\mathbf{M}}_\mathbf{1}&\left(\hat{\mathbf{C}}_\mathbf{1}(\upsilon,\omega)\upsilon + \hat{\mathbf{D}}_\mathbf{1}(\upsilon)\upsilon + \hat{\mathbf{g}}_\mathbf{1}(\eta_2)\right) - \hat{\mathbf{M}}_\mathbf{1}\hat{d}_1 \\ &+ \hat{\mathbf{M}}_\mathbf{1}(\dot{\alpha}_1 - \beta_1\mathbf{z}_3) - 2\hat{\mathbf{M}}_\mathbf{1}\frac{\partial V_1}{\partial\|\mathbf{z}_{a1}\|^2}\mathbf{R}_E^B\mathbf{z}_{a1} \end{aligned} \tag{24}$$

$$\begin{aligned} \tau_2 = \hat{\mathbf{M}}_\mathbf{2}&\left(\hat{\mathbf{C}}_\mathbf{2}(\upsilon,\omega)\omega + \hat{\mathbf{D}}_\mathbf{2}(\omega)\omega + \hat{\mathbf{g}}_\mathbf{2}(\eta_2)\right) - \hat{\mathbf{M}}_\mathbf{2}\hat{d}_2 \\ &+ \hat{\mathbf{M}}_\mathbf{2}(\dot{\alpha}_2 - \beta_2\mathbf{z_4}) - 2\hat{\mathbf{M}}_\mathbf{2}\frac{\partial V_2}{\partial\|\mathbf{z}_2\|^2}R_2^T\mathbf{z}_2 \end{aligned} \tag{25}$$

where β_1 and β_2 are positive design parameters chosen to be greater than $1/4$. Then, all the signals in the closed-loop system are bounded, and the constraints for DBCD and attitude tracking error in each DOF hold.

Proof. The derivative of the Lyapunov function V_T (23) with respect to time, is

$$\dot{V}_T = \mathbf{z_3^T}\dot{\mathbf{z}}_\mathbf{3} + \mathbf{z_4^T}\dot{\mathbf{z}}_\mathbf{4} + \dot{\mathbf{V}}_\mathbf{1} + \dot{\mathbf{V}}_\mathbf{2} \tag{26}$$

Also, substituting the time-derivative of the error variables $\mathbf{z}_3$ and $\mathbf{z}_4$, and (14) into (26) gives

$$\begin{aligned} \dot{V}_T = &\mathbf{z}_3^T\left(\tilde{\mathbf{d}}_1 - \beta_1\mathbf{z}_3 - 2\frac{\partial V_1}{\partial\|\mathbf{z}_1\|^2}\mathbf{R}_E^B\mathbf{z}_{a1}\right) \\ &+ \mathbf{z}_4^T\left(\tilde{\mathbf{d}}_2 - \beta_2\mathbf{z}_4 - 2\frac{\partial V_2}{\partial\|\mathbf{z}_2\|^2}\mathbf{R}_2^T\mathbf{z}_2\right) - V_1 \\ &+ 2\left(\frac{\partial}{\partial\|\mathbf{z}_{a1}\|^2}V_1\right)\mathbf{z}_{a1}^T\mathbf{R}_B^E\mathbf{z}_3 - \left(\frac{\partial}{\partial\|\mathbf{z}_{a1}\|^2}V_1\right)^2\mathbf{z}_{a1}^T\mathbf{z}_{a1} \\ &+ 2\frac{\partial V_2}{\partial\|\mathbf{z}_2\|^2}\mathbf{z}_2^T\mathbf{R}_2\mathbf{z}_4 - V_2 - \sum_{i=1}^{3}\left(\frac{\partial V_2}{\partial\mathbf{z}_{2i}^2}\right)^2\mathbf{z}_{2i}^2 \end{aligned} \tag{27}$$

Substituting the control law (24) and (25) into (27), gives:

$$\begin{aligned} \dot{V}_T = &\mathbf{z}_3^T\left(\tilde{\mathbf{d}}_1 - \beta_1\mathbf{z}_3 - 2\frac{\partial V_1}{\partial\|\mathbf{z}_{a1}\|^2}\mathbf{R}_E^B\mathbf{z}_{a1}\right) \\ &+ \mathbf{z}_4^T\left(\tilde{\mathbf{d}}_2 - \beta_2\mathbf{z}_4 - 2\frac{\partial V_2}{\partial\|\mathbf{z}_2\|^2}\mathbf{R}_2^T\mathbf{z}_2\right) \\ &- V_1 + 2\left(\frac{\partial}{\partial\|\mathbf{z}_{a1}\|^2}V_1\right)\mathbf{z}_{a1}^T\mathbf{R}_B^E\mathbf{z}_3 \\ &- \left(\frac{\partial}{\partial\|\mathbf{z}_{a1}\|^2}V_1\right)^2\mathbf{z}_{a1}^T\mathbf{z}_{a1} - V_2 \\ &+ 2\frac{\partial V_2}{\partial\|\mathbf{z}_2\|^2}\mathbf{z}_2^T\mathbf{R}_2\mathbf{z}_4 - \sum_{i=1}^{3}\left(\frac{\partial V_2}{\partial\mathbf{z}_{2i}^2}\right)^2\mathbf{z}_{2i}^2 \end{aligned} \tag{28}$$

By Youngs inequality, $\mathbf{z}_3^T\tilde{\mathbf{d}}_1 \le \frac{1}{4}\|\mathbf{z}_3\|^2 + \left\|\tilde{\mathbf{d}}_1\right\|^2$, and, in a similar way, $\mathbf{z}_4^T\tilde{\mathbf{d}}_2 \le \frac{1}{4}\|\mathbf{z}_4\|^2 + \left\|\tilde{\mathbf{d}}_2\right\|^2$. Also it is routine to establish that

$$\left(\frac{\partial}{\partial\|\mathbf{z}_{a1}\|^2}V_1\right)\mathbf{z}_{a1}^T\mathbf{R}_B^E\mathbf{z}_3 = \mathbf{z}_3^T\frac{\partial V_1}{\partial\|\mathbf{z}_{a1}\|^2}\mathbf{R}_E^B\mathbf{z}_{a1} \tag{29}$$

$$\frac{\partial V_2}{\partial\|\mathbf{z}_2\|^2}\mathbf{z}_2^T\mathbf{R}_2\mathbf{z}_4 = \mathbf{z}_4^T\frac{\partial V_2}{\partial\|\mathbf{z}_2\|^2}\mathbf{R}_2^T\mathbf{z}_2 \tag{30}$$

and the derivative of the Lyapunov function V_T is further simplified to

$$\begin{aligned}\dot{V}_T \leq & -\left(\beta_1-\frac{1}{4}\right)\|\mathbf{z}_3\|^2-\left(\beta_2-\frac{1}{4}\right)\|\mathbf{z}_4\|^2 \\ & +\left\|\tilde{\mathbf{d}}_1\right\|^2+\left\|\tilde{\mathbf{d}}_2\right\|^2 \\ & -V_1-V_2-\left(\frac{\partial}{\partial\|\mathbf{z}_{a1}\|^2}V_1\right)^2\mathbf{z}_{a1}^T\mathbf{z}_{a1}-\sum_{i=1}^{3}\left(\frac{\partial V_2}{\partial \mathbf{z}_{2i}^2}\right)^2\mathbf{z}_{2i}^2 \\ & \leq -\mu_1 V_T+\Delta_1 \end{aligned} \tag{31}$$

where $\mu_1 = \min\left\{\left(\beta_1-\frac{1}{4}\right),\left(\beta_2-\frac{1}{4}\right),1\right\}$, and Δ_1 is the bound of the sum of $\left\|\tilde{\mathbf{d}}_1\right\|^2$ and $\left\|\tilde{\mathbf{d}}_2\right\|^2$ after a certain time. This conclusion relies on the fact that the estimated errors $\left\|\tilde{\mathbf{d}}_1\right\|^2$ and $\left\|\tilde{\mathbf{d}}_2\right\|^2$ can be shown to be finite-time convergent, for full background on this property see, e.g., [24].

Multiplying both sides of (31) by $exp(\mu_1 t)$, gives, after some routine manipulations,

$$\begin{aligned} V_T &\leq V_T(0)\exp(-\mu_1 t)-\Delta_1(\exp(-\mu_1 t)-1) \\ &\leq \max\{V_T(0),\Delta_1\} \end{aligned} \tag{32}$$

Using (32), it follows that all the signals in the closed-loop system are bounded. Also the definition of the Lyapunov functions (5), (9) and (23), gives that $\varepsilon_{1b} < \|\mathbf{z}_{a1}\|^2 < \varepsilon_{1a}$ and $0 < \mathbf{z}_{2i}^2 < \varepsilon_{2a}$. Therefore, under this control scheme, the distance DBCD is guaranteed to be always within the prescribed lower and upper boundaries, while the absolute value of the attitude tracking error in each DOF is also less than the prescribed bound. □

Remark 3. *In previous barrier Lyapunov function-based control schemes, the DBCD will converge to zero and within the prescribed boundaries. Under the design in this paper, the DBCD cannot converge to zero due to the introduction of a lower boundary, with the consequent property of reduced control effort, which can also be adjusted from application to application by varying the boundary value. Moreover, the general uncertainties are estimated by an observer with the finite-time convergence property, reducing the computational effort needed.*

IV. Simulation case studies

This section first gives the results of a numerical study of the application of the new design to an open-frame underwater vehicle known as ODIN AUV. Also, the results obtained are compared with those of two existing designs.

This vehicle is fully-actuated, and its physical parameters are given in [25]. Moreover, due to its structure, the vehicle's roll and pitch angles are always kept within a small range of zero. Therefore, these angles are not controlled in this paper, and the initial conditions of the vehicle are taken as $\eta(0) = \left[1.0,-1.0,-1.4,\frac{\pi}{18},-\frac{\pi}{18},\frac{\pi}{9}\right]^T$ and $\dot{\eta}(0) = [-0.04,0.04,-0.04,0.02,-0.02,0.02]^T$. Also, 60% modeling uncertainties are considered, i.e., the physical parameters of the vehicle used to design the controller could vary from their true values by up to 40%.

External disturbances, including the ocean current and others, are also simulated, where the magnitude of the ocean current is generated by a first-order Markov equation [22]. Here, the mean magnitude of the ocean current is $0.504m/s$, and its standard deviation is $0.084m/s$. In general, the generated ocean current is irrotational, i.e., the ocean current $\upsilon_{\mathbf{c}} = [u_c, v_c, w_c, 0, 0, 0]^T$, where u_c, v_c, w_c are the projections of the magnitude V_C. Specifically, $u_c = V_C\cos(\alpha_c)\cos(\beta_c)$,$v_c = V_C\sin(\beta_c)$ and $u_c = V_C\sin(\alpha_c)\cos(\beta_c)$, where α_c and β_c are the angle of attack and the sideslip angle, respectively, simulated by the sum of a Gaussian noise function.

The ocean current $\upsilon_{\mathbf{c}}$ is described in the body-fixed frame and introduced into ODIN AUV as relative velocity in [26]. Moreover, the other external disturbance τ_{ed1} and τ_{ed2} are simulated as $\tau_{ed1} = [\tau_{ed11},\tau_{ed12},\tau_{ed13}]^T$ with $\tau_{ed11} = 2rand + 4\sin(0.3t)$, $\tau_{ed12} = 2rand + 8\sin(0.2t)$, $\tau_{ed13} = 2rand + 6\sin(0.1t)$ and $\tau_{ed2} = 2rand + 8\cos(0.3t)$, where rand denotes a random number generator [27].

In the control scheme developed in the previous section, the performance bound width affects the variation of control signals. Specifically, if the bound width increases, the variation of the control signals will decrease. However, the performance bound width is determined by the given task for the underwater vehicle, e.g., limited communication range or the detection range of the sensors used.

A 3-D Dubins trajectory is chosen as the desired trajectory $\eta_d = [x_d, y_d, z_d, \phi_d]$, where

$$x_d = \begin{cases} 0, 0\leq t<20 \\ 0.2(t-20), 20\leq t<40 \\ \sin(0.05\pi(t-40))+4, 40\leq t<60 \\ -0.2(t-60)+4, 60\leq t<80 \\ -\sin(0.05\pi(t-80)), 80\leq t<100 \\ 0.2(t-100), 100\leq t<120 \\ \sin(0.05\pi(t-120))+4, 120\leq t<140 \\ -0.2(t-140)+4, 140\leq t<160 \\ -\sin(0.05\pi(t-160)), 160\leq t<180 \\ 0.2(t-180), 180\leq t<200 \end{cases}$$

$$y_d = \begin{cases} 1, 0\leq t<20 \\ 1, 20\leq t<40 \\ -\cos(0.05\pi(t-40))+2, 40\leq t<60 \\ 3, 60\leq t<80 \\ -\cos(0.05\pi(t-80))+4, 80\leq t<100 \\ 5, 100\leq t<120 \\ -\cos(0.05\pi(t-120))+6, 120\leq t<140 \\ 7, 140\leq t<160 \\ -\cos(0.05\pi(t-160))+8, 160\leq t<180 \\ 9, 180\leq t<200 \end{cases}$$

$$\phi_d = \begin{cases} 0, 0 \le t < 40 \\ 0.5\pi\left(1-\cos\left(0.05\pi\left(t-40\right)\right)\right), 40 \le t < 60 \\ \pi, 60 \le t < 80 \\ \pi - 0.5\pi\left(1-\cos\left(0.05\pi\left(t-80\right)\right)\right), 80 \le t < 100 \\ 0, 100 \le t < 120 \\ 0.5\pi\left(1-\cos\left(0.05\pi\left(t-120\right)\right)\right), 120 \le t < 140 \\ \pi, 140 \le t < 160 \\ \pi - 0.5\pi\left(1-\cos\left(0.05\pi\left(t-160\right)\right)\right), 160 \le t < 180 \\ 0, 180 \le t < 200 \end{cases}$$

$$z_d = -2, 0 \le t \le 200 \tag{33}$$

To provide a comparison, two existing region tracking control strategies are also considered. The first of these is the adaptive region boundary-based control strategy developed in [9] and combined with a RBF neural network in [20], denoted as Comparison A, for which the controller is

$$\begin{aligned} f_{b1} &= \frac{1}{2}\left(\left(\eta_1-\eta_{d1}\right)^T\left(\eta_1-\eta_{d1}\right)-\delta_a^2\right) \\ f_{b2} &= \frac{1}{2}\sum_{i=1}^{3}\left(\left(\eta_2\left(i\right)-\eta_{d2}\left(i\right)\right)^2-\delta_b^2\right) \\ \Delta\xi_a &= \kappa\max\left(0,f_{b1}\right)\left(\eta_1-\eta_{d1}\right) \\ \Delta\xi_b &= \kappa diag\left\{\max\left(0,f_{b2}\right)\right\}\left(\eta_2-\eta_{d2}\right) \\ \upsilon_s &= J^{-1}\left(\eta\right)\left(col\left(\dot\eta_{d1},\dot\eta_{d2}\right)-col\left(\Delta\xi_a,\Delta\xi_b\right)\right) \\ u &= B^+\left(-\hat W\Phi\left(\upsilon\right)-M\dot\upsilon_s-K_d\tilde\upsilon\right) \\ &\quad -B^+\left(J^T\left(\eta\right)K_p col\left(\Delta\xi_a,\Delta\xi_b\right)+k_s sign\left(\tilde\upsilon\right)\right) \end{aligned} \tag{34}$$

where $\tilde\upsilon=\upsilon-\upsilon_s$, δ_a,δ_b,κ and k_s are positive constants, and $\hat W\Phi\left(\upsilon\right)$ is the output of the RBF neural network as in [20]. Also, the adaptive rate of the weighting matrix $\hat W$ is the same as in [20].

The second comparative control strategy is from [26], where only the steady-state performance of the region tracking for each DOF is considered, denoted as Comparison B, with controller

$$\begin{aligned} u &= \mathbf{B}^+\mathbf{J}^T\left(\Theta-\hat\rho_3\left\|\Theta\right\|\mathrm{sgn}_{\varepsilon 2}(\mathbf{z}_2)\right) \\ &\quad -\mathbf{B}^+\mathbf{J}^T\hat{\mathbf{M}}_\eta(\hat\rho_0+\hat\rho_1\left\|\dot\eta\right\|+\hat\rho_2\|\dot\eta\|^2)\mathrm{sgn}_{\varepsilon 2}(\mathbf{z}_2) \\ \dot{\hat\rho}_0 &= \Gamma_0\left(k\mathbf{P}_{2,\varepsilon 2}(\mathbf{z}_2)+\mathbf{P}_{1,\varepsilon 2}(\mathbf{z}_2)\right) \\ \dot{\hat\rho}_1 &= \Gamma_1\left(k\mathbf{P}_{2,\varepsilon 2}(\mathbf{z}_2)+\mathbf{P}_{1,\varepsilon 2}(\mathbf{z}_2)\right)\left\|\dot\eta\right\| \\ \dot{\hat\rho}_2 &= \Gamma_2\left(k\mathbf{P}_{2,\varepsilon 2}(\mathbf{z}_2)+\mathbf{P}_{1,\varepsilon 2}(\mathbf{z}_2)\right)\left\|\dot\eta\right\|^2 \\ \dot{\hat\rho}_3 &= \Gamma_3\hat{\mathbf{M}}_\eta^{-1}\left(k\mathbf{P}_{2,\varepsilon 2}(\mathbf{z}_2)+\mathbf{P}_{1,\varepsilon 2}(\mathbf{z}_2)\right)\left\|\Theta\right\| \\ \Theta &= \hat{\mathbf{M}}_\eta\dot\alpha_1-(g_2+1)\hat{\mathbf{M}}_\eta\mathbf{P}_{1,\varepsilon 2}(\mathbf{z}_2)\mathrm{sgn}_{\varepsilon 2}(\mathbf{z}_2) \\ &\quad +\hat{\mathbf{C}}_\eta\dot\eta+\hat{\mathbf{D}}_\eta\dot\eta+\hat{\mathbf{g}}_\eta \\ \alpha_1 &= -(g_1+\frac{1}{4})(k\mathbf{P}_{3,\varepsilon_1}(\mathbf{z}_1)+\mathbf{P}_{2,\varepsilon_1}(\mathbf{z}_1))\mathrm{sgn}_{\varepsilon_1}(\mathbf{z}_1) \\ &\quad +\dot\eta_R-(\varepsilon_2+\sigma)\mathrm{sgn}_{\varepsilon_1}(\mathbf{z}_1) \end{aligned} \tag{35}$$

where η_R is the desired trajectory, $\mathbf{z}_1=\eta-\eta_R$ and $\mathbf{z}_2=\dot\eta-\alpha_1$; $\hat{\mathbf{M}}_\eta$, $\hat{\mathbf{C}}_\eta$, $\hat{\mathbf{D}}_\eta$, $\hat{\mathbf{g}}_\eta$ are the dynamics of the vehicle described in the earth frame, which are given in [26]. The matrices $\mathbf{P}_{2,\varepsilon 2}(\mathbf{z}_2)$, $\mathbf{P}_{1,\varepsilon 2}(\mathbf{z}_2)$, $\mathbf{P}_{3,\varepsilon_1}(\mathbf{z}_1)$ and $\mathbf{P}_{2,\varepsilon_1}(\mathbf{z}_1)$ and the vectors $\mathrm{sgn}_{\varepsilon 2}(\mathbf{z}_2)$ and $\mathrm{sgn}_{\varepsilon_1}(\mathbf{z}_1)$ are the same as those in [26].

The control strategy is the same as that in [26]. It should be noted that the control strategy in [26] focuses on the region tracking performance of each DOF, but the new design developed in this paper investigates the sphere region tracking performance.

To enable a fair comparison between designs, the boundaries of the tracking error in the X, Y, and Z directions are $\frac{\sqrt{3}}{6}$ for each design. Note that the norm of the position tracking error is less than 0.5 if the absolute values of all the tracking errors for X, Y, and Z directions are less than $\frac{\sqrt{3}}{6}$. The prescribed boundary for the yaw tracking error is the same as that for the new control scheme, i.e., 0.1 rad.

The controller parameters for each design used to generate the simulation results given and discussed below are in TABLE I.

TABLE I
PARAMETERS FOR DIFFERENT CONTROLLERS

Controller	Control parameters
This paper	$\rho_{01}=3,\rho_{\infty 1}=0.5,\lambda_1=0.1,\varepsilon_{1b}=0.09,$ $\rho_{02}=0.5,\rho_{\infty 2}=0.1,\beta_1=\beta_2=0.3,$ $k_1=p_1=0.3,k_2=p_2=2.1,\lambda_2=0.1,$ $k_3=p_3=1.1,k_4=p_4=1.21.$
Comparison A	$\delta_a=0.5,\delta_b=0.1,\kappa=5,k_s=5,$ $K_d=diag\left(50,50,50,30\right),$ $K_p=100\times diag\left(50,50,50,15\right).$
Comparison B	$\varepsilon_1=[\frac{\sqrt{3}}{6},\frac{\sqrt{3}}{6},\frac{\sqrt{3}}{6},0.1]^T,g_1=2,$ $\varepsilon_2=[0.3,0.3,0.3,0.3]^T,g_2=5,$ $\Gamma_0=\Gamma_1=\Gamma_2=0.1\times diag\left(1,1,1,0.1\right),$ $\Gamma_3=0.01\times diag\left(1,1,1,0.1\right),k=1.$

The results for the design developed in this paper are given in Figs. 3, 4 and 5, where Fig. 5b only shows one of the control signals to the vertical thrusters, i.e., for the vertical thruster (T_5), since the other three vertical thrusters have the same control signals as T_5. Fig. 4 gives the norm of the position tracking error, i.e., the distance from the AUV position to the corresponding point on the desired trajectory. The bottom plot in this figure shows the absolute value of the yaw tracking error. It is concluded from Fig. 4 that the norm of the position tracking error always remains within the prescribed boundaries. At the same time, the yaw tracking error also always remains within the predesigned limits. The tracking error on each DOF is given in Fig. 5a and Fig. 5b shows the corresponding control input to each thruster.

The results in Fig. 4 demonstrate the successful implementation of the new control scheme. Although the tracking errors in the X, Y, and Z directions vary within a range close to zero and do not converge to zero (see Fig. 5a), this is as expected since high tracking precision is not the control objective in this paper. In particular, the controller is successful if the norm

of the position tracking error is always within the prescribed boundaries and the absolute value of the yaw tracking error is less than the predesigned boundary.

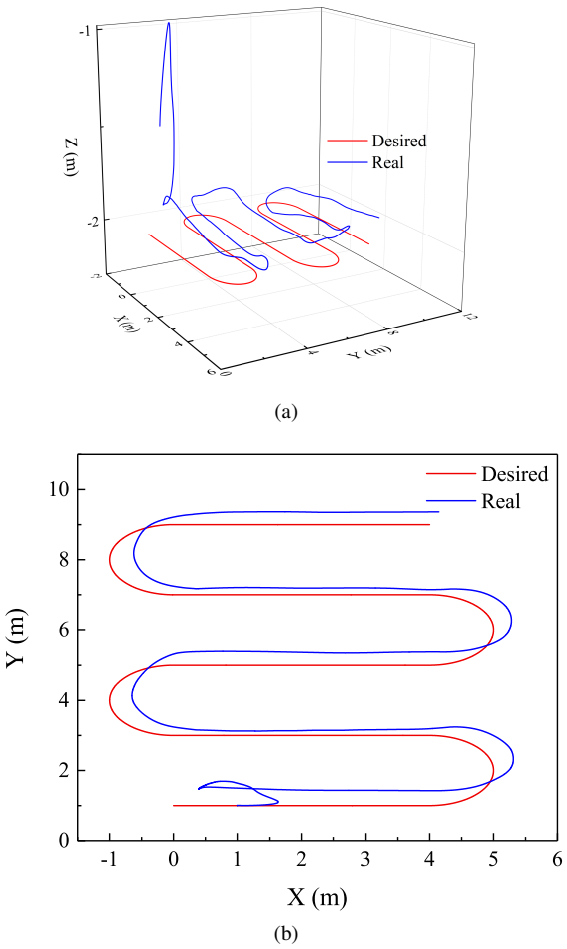

Fig. 3. Desired and generated trajectories: (a) XYZ plot of AUV and desired trajectory, (b) XY plot.

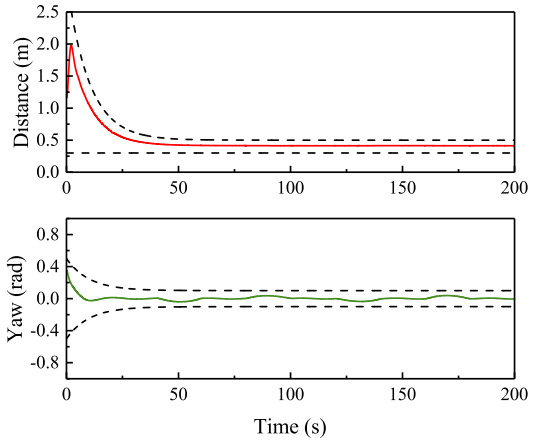

Fig. 4. Region tracking performance of the new control design.

Comparative control scheme A also focuses on the region tracking of the norm of the position tracking error during the steady state. Figs. 6 and 7 give the simulation results.

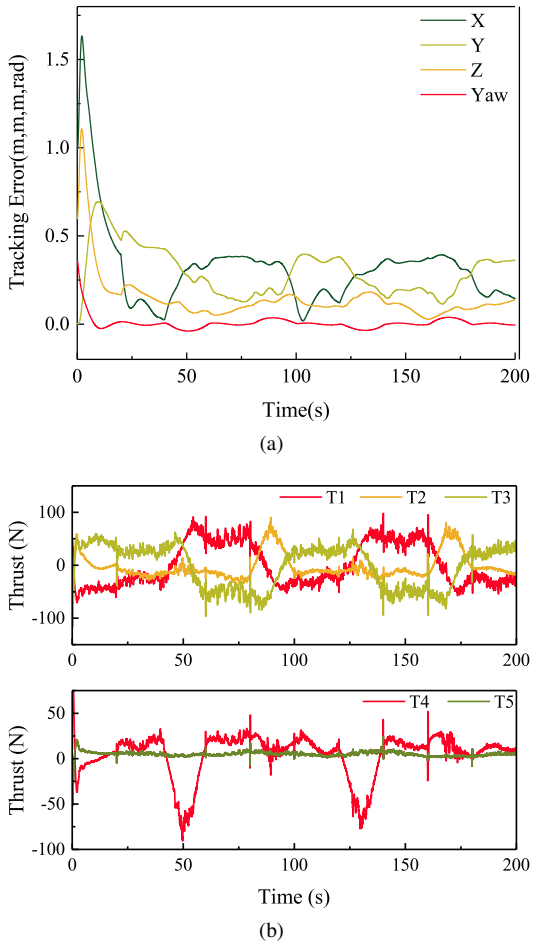

Fig. 5. Tracking results based for the new control scheme: (a) Tracking error, (b) Control input, where $T_i, i = 1, 2, \ldots, 5$, denotes the control inputs for the thrusters.

Similarly, Fig. 6 shows the norm of the position tracking error and the absolute value of the yaw tracking error, respectively. The tracking error on each DOF and the corresponding control inputs to the thrusters are shown in Fig. 7. From Fig. 6, it is evident that the norm of the position tracking error during the steady stage is larger than the prescribed boundary $(0.5m)$, while the yaw angle error also violates the prescribed limits. These simulation results confirm that the control objective in this paper is not achieved by the region tracking control scheme in [9].

Comparative design B was developed to drive the tracking error on each DOF during the steady stage to be within the prescribed boundaries rather than focusing on the norm of the position tracking error. The tracking results for this design are given in Figs. 8 and 9. Fig. 8 gives the norm of the position tracking error and the absolute value of the yaw tracking error, respectively. From Fig. 8, it can be seen that the norm of the position tracking error can be quickly driven into the prescribed boundary, i.e., $0.5m$. However, it can also be seen that the absolute value of the yaw tracking error cannot be maintained within the specified boundary, i.e., $0.1rad$, after it first enters.

In [26], the desired yaw angle was fixed, and the tracking performance requirement for the yaw angle was satisfied.

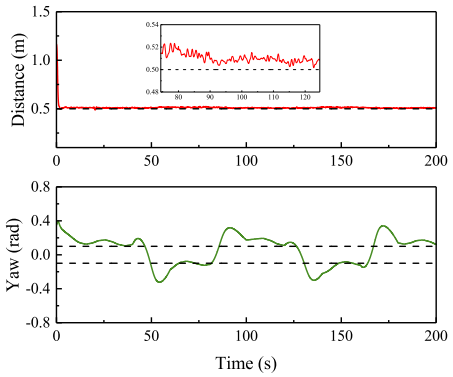

Fig. 6. Region tracking performance using comparative control scheme A.

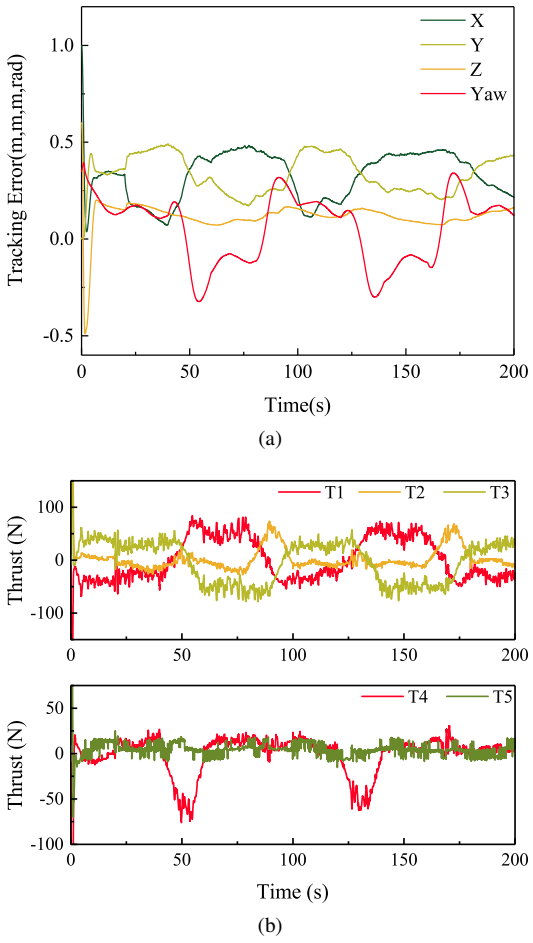

Fig. 7. Tracking results for comparative control scheme A: (a) tracking error. (b) control input.

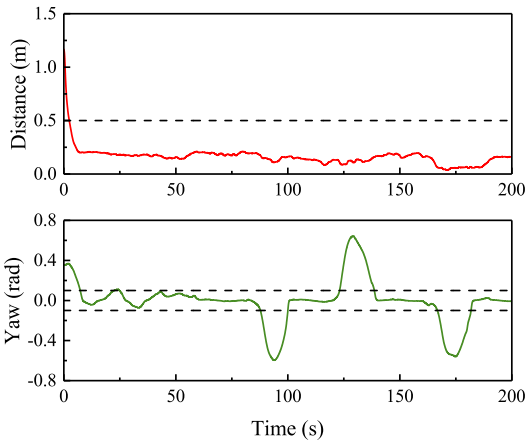

Fig. 8. Region tracking performance for comparative control scheme B.

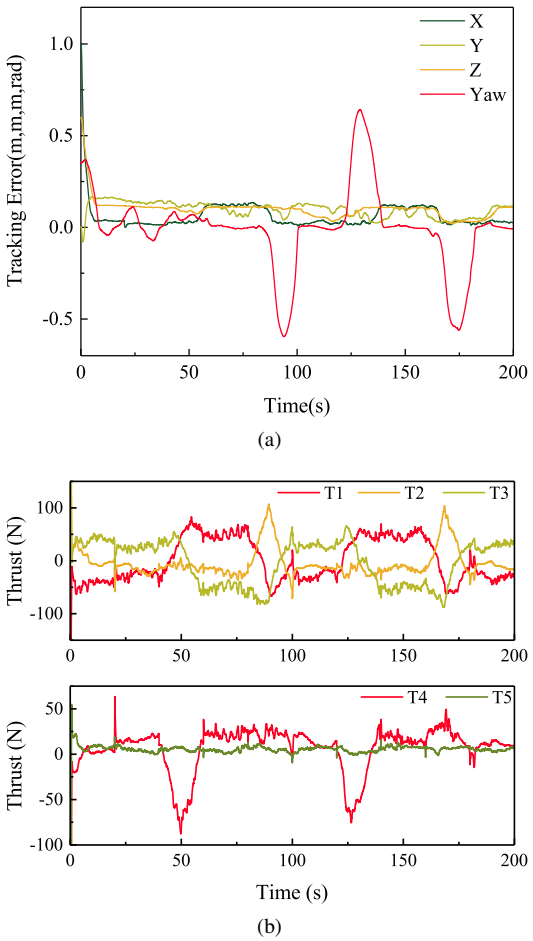

Fig. 9. Tracking results for comparative control scheme B: (a) tracking error. (b) control input.

However, the desired yaw angle is time-varying, and more strict requirements are required in the controller. From Figs. 8 and 9, it is concluded that the controller cannot follow the time-varying yaw angle quickly and significantly violates its prescribed boundary, especially when the desired yaw angle changes. Fig. 9 shows the tracking error for each DOF and the corresponding control input of each thruster.

From the simulation results for the three designs, only the new design developed in this paper satisfies the overall control objectives, i. e. the norm of the position tracking error is within the prescribed boundary in the steady state and the absolute value of the yaw tracking error is less than the predesigned value. However, the control input to each thruster shown in Fig. 9b has less high-frequency fluctuation than in Fig. 5b. One area for possible future research is how to enhance the design to reduce the high-frequency fluctuation in the control input of each thruster.

V. Conclusions and Further Research

This paper has investigated the region tracking problem, especially the norm of the position tracking error for an underwater vehicle. A novel region-tracking control scheme has been developed based on two forms of barrier Lyapunov functions and an observer designed to estimate the general uncertainty. Also, a detailed numerical performance study has demonstrated that the new control scheme can guarantee that the norm of the position tracking error will always be within the prescribed boundaries. Moreover, the absolute value of the yaw angle is always less than the predesigned value.

It has been demonstrated that the new design outperforms two previously reported designs using the results of a simulation study. Such results are a necessary step to proceed to experimental validation. Future research will investigate how to reduce the high-frequency fluctuations in the control inputs for the new design that may (potentially) be problematic for some applications and region-tracking control schemes for under-actuated underwater vehicles.

References

[1] A. A. RedwanNewaz, T. Alam, G. Murad Reis, L. Bobadilla, and R. N. Smith, "Long-term autonomy for auvs operating under uncertainties in dynamic marine environments," *IEEE Robotics and Automation Letters*, vol. 6, no. 4, pp. 6313–6320, 2021.

[2] Y. Zhang, B. Kieft, B. W. Hobson, J. P. Ryan, B. Barone, C. M. Preston, B. Roman, B.-Y. Raanan, R. Marin, T. C. O'Reilly, C. A. Rueda, D. Pargett, K. M. Yamahara, S. Poulos, A. Romano, G. Foreman, H. Ramm, S. T. Wilson, E. F. DeLong, D. M. Karl, J. M. Birch, J. G. Bellingham, and C. A. Scholin, "Autonomous tracking and sampling of the deep chlorophyll maximum layer in an open-ocean eddy by a long-range autonomous underwater vehicle," *IEEE Journal of Oceanic Engineering*, vol. 45, no. 4, pp. 1308–1321, 2020.

[3] X. Wang and C. P. Tan, "Dynamic output feedback fault tolerant control for unmanned underwater vehicles," *IEEE Transactions on Vehicular Technology*, vol. 69, no. 4, pp. 3693–3702, 2020.

[4] D. Debruyn, R. Zufferey, S. F. Armanini, C. Winston, A. Farinha, Y. Jin, and M. Kovac, "Medusa: a multi-environment dual-robot for underwater sample acquisition," *IEEE Robotics and Automation Letters*, pp. 1–1, 2020.

[5] F. Sedghi, M. M. Arefi, A. Abooee, and O. Kaynak, "Adaptive robust finite-time nonlinear control of a typical autonomous underwater vehicle with saturated inputs and uncertainties," *IEEE/ASME Transactions on Mechatronics*, pp. 1–1, 2020.

[6] Y. Zhang, X. Liu, M. Luo, and C. Yang, "Bio-inspired approach for long-range underwater navigation using model predictive control," *IEEE Trans Cybern*, vol. 51, no. 8, pp. 4286–4297, 2021.

[7] Z. Yan, P. Gong, W. Zhang, and W. Wu, "Model predictive control of autonomous underwater vehicles for trajectory tracking with external disturbances," *Ocean Engineering*, vol. 217, 2020.

[8] C. Yu, X. Xiang, P. A. Wilson, and Q. Zhang, "Guidance-error-based robust fuzzy adaptive control for bottom following of a flight-style auv with saturated actuator dynamics," *IEEE Transactions on Cybernetics*, vol. 50, no. 5, pp. 1887–1899, 2020.

[9] Z. H. Ismail and M. W. Dunnigan, "Tracking control scheme for an underwater vehicle-manipulator system with single and multiple sub-regions and sub-task objectives," *IET Control Theory & Applications*, vol. 5, no. 5, pp. 721–735, 2011.

[10] S. L. Dai, S. He, M. Wang, and C. Yuan, "Adaptive neural control of underactuated surface vessels with prescribed performance guarantees," *IEEE Trans Neural Netw Learn Syst*, vol. 30, no. 12, pp. 3686–3698, 2019. [Online]. Available: https://www.ncbi.nlm.nih.gov/pubmed/30418926

[11] O. Elhaki, K. Shojaei, and P. Mehrmohammadi, "Reinforcement learning-based saturated adaptive robust neural-network control of underactuated autonomous underwater vehicles," *Expert Systems with Applications*, vol. 197, 2022.

[12] R. Rout, R. Cui, and Z. Han, "Modified line-of-sight guidance law with adaptive neural network control of underactuated marine vehicles with state and input constraints," *IEEE Transactions on Control Systems Technology*, pp. 1–13, 2020.

[13] K. Shojaei and A. Chatraei, "Robust platoon control of underactuated autonomous underwater vehicles subjected to nonlinearities, uncertainties and range and angle constraints," *Applied Ocean Research*, vol. 110, 2021.

[14] C. P. Bechlioulis and G. A. Rovithakis, "A low-complexity global approximation-free control scheme with prescribed performance for unknown pure feedback systems," *Automatica*, vol. 50, no. 4, pp. 1217–1226, 2014.

[15] L. Chen and H. Yang, "Adaptive neural prescribed performance output feedback control of pure feedback nonlinear systems using disturbance observer," *International Journal of Adaptive Control and Signal Processing*, vol. 34, no. 4, pp. 520–542, 2020.

[16] J. X. Zhang and G. H. Yang, "Prescribed performance fault-tolerant control of uncertain nonlinear systems with unknown control directions," *IEEE Transactions on Automatic Control*, vol. 62, no. 12, pp. 6529–6535, 2017.

[17] H. Liang, Y. Fu, J. Gao, and H. Cao, "Finite-time velocity-observed based adaptive output-feedback trajectory tracking formation control for underactuated unmanned underwater vehicles with prescribed transient performance," *Ocean Engineering*, vol. 233, 2021.

[18] H. Liu, Y. Wang, and F. L. Lewis, "Robust distributed formation controller design for a group of unmanned underwater vehicles," *IEEE Transactions on Systems, Man, and Cybernetics: Systems*, vol. 51, no. 2, pp. 1215–1223, 2021.

[19] X. Liu, M. Zhang, and S. Wang, "Adaptive region tracking control with prescribed transient performance for autonomous underwater vehicle with thruster fault," *Ocean Engineering*, vol. 196, p. 106804, 2020.

[20] X. Liu, M. Zhang, F. Yao, B. Yin, and J. Chen, "Barrier lyapunov function based adaptive region tracking control for underwater vehicles with thruster saturation and dead zone," *Journal of the Franklin Institute*, vol. 358, no. 11, pp. 5820–5844, 2021.

[21] X. Liu, M. Zhang, and E. Rogers, "Trajectory tracking control for autonomous underwater vehicles based on fuzzy re-planning of a local desired trajectory," *IEEE Transactions on Vehicular Technology*, vol. 68, no. 12, pp. 11 657–11 667, 2019.

[22] T. I. Fossen, *Handbook of marine craft hydrodynamics and motion control*. New York: John Wiley & Sons, 2011.

[23] R. Rout and B. Subudhi, "Narmax self-tuning controller for line-of-sight-based waypoint tracking for an autonomous underwater vehicle," *IEEE Transactions on Control Systems Technology*, vol. 25, no. 4, pp. 1529–1536, 2017.

[24] J. A. Moreno and M. Osorio, "A lyapunov approach to second-order sliding mode controllers and observers," in *2008 47th IEEE Conference on Decision and Control*, 2008, Conference Proceedings, pp. 2856–2861.

[25] L. Qiao and W. Zhang, "Adaptive second-order fast nonsingular terminal sliding mode tracking control for fully actuated autonomous underwater vehicles," *IEEE Journal of Oceanic Engineering*, vol. 44, no. 2, pp. 363–385, 2019.

[26] M. Zhang, X. Liu, and F. Wang, "Backstepping based adaptive region tracking fault tolerant control for autonomous underwater vehicles," *Journal of Navigation*, vol. 70, no. 1, pp. 184–204, 2017.

[27] L. Qiao and W. Zhang, "Trajectory tracking control of auvs via adaptive fast nonsingular integral terminal sliding mode control," *IEEE Transactions on Industrial Informatics*, vol. 16, no. 2, pp. 1248–1258, 2020.